Optics Letters

Quantum delayed-choice experiment with a single neutral atom

Gang Li,[1,2,*] Pengfei Zhang,[1,2] and Tiancai Zhang[1,2]

[1]State Key Laboratory of Quantum Optics and Quantum Optics Devices, and Institute of Opto-Electronics, Shanxi University, Taiyuan 030006, China
[2]Collaborative Innovation Center of Extreme Optics, Shanxi University, Taiyuan 030006, China
*Corresponding author: gangli@sxu.edu.cn

Received 20 July 2017; accepted 23 August 2017; posted 31 August 2017 (Doc. ID 302840); published 21 September 2017

We present a proposal to implement a quantum delayed-choice (QDC) experiment with a single neutral atom, such as a rubidium or cesium atom. In our proposal, a Ramsey interferometer is adopted to observe the wave-like or particle-like behaviors of a single atom depending on the existence or absence of the second $\pi/2$-rotation. A quantum-controlled $\pi/2$-rotation on target atom is realized through a Rydberg-Rydberg interaction by another ancilla atom. It shows that a heavy neutral atom can also have a morphing behavior between the particle and the wave. The realization of the QDC experiment with such heavy neutral atoms not only is significant to understand the Bohr's complementarity principle in matter-wave and matter-particle domains but also has great potential on the quantum information process with neutral atoms.

OCIS codes: (000.1600) Classical and quantum physics; (270.0270) Quantum optics.

https://doi.org/10.1364/OL.42.003800

Wave-like and particle-like behaviors are two distinct and incompatible natures for a quantum particle in the view of classical physics. A quantum particle can show either wave-like behavior or particle-like behavior, depending on the measurement arrangement. For example, to study the nature of a photon, which is a massless particle, a Mach–Zehnder interferometer (MZI) is usually adapted [see Fig. 1(a)]. In such a MZI, an input photon is first split by a beam splitter (BS_1) and travels along the two paths, where the phase shift ϕ between these two paths is tunable. The photon is then recombined by BS_2 and finally detected. By inserting BS_2 into the MZI, the interference between the two paths can be observed by both detectors, D_1 and D_2, which means that the photon takes two paths simultaneously and shows wave-like behavior. However, when BS_2 is removed, the photon will be detected by only one of the detectors with equal probability 1/2, which reveals that the photon takes only one of the two paths and, finally, shows particle-like behavior. Due to the two measurement arrangements being mutually exclusive, the wave-like behavior and the particle-like behavior cannot be simultaneously observed [1–4]. Such an exhibition of wave-particle duality for a photon is a good illustration of Bohr's complementarity principle (BCP).

In the same setup, it was argued that the photon could know in advance whether to take one path or both paths depending on the absence or existence of BS_2 via a hidden variable and, thus, decides which behavior to show. This casual standpoint is precluded by Wheeler's delayed-choice experiment [4–7]. In this Gedanken experiment, the second BS_2 is chosen to randomly appear or disappear in the MZI after the photon has entered the interferometer. Thus, the photon could not get the information in advance about which measuring arrangement it will encounter. The implementations of Wheeler's experiment with a photon have been demonstrated not only in the context of a wave-particle property [8–10], but also in the context of the entanglement-separation property [11]. The more meaningful experiments with matter particles, such as electrons and atom, have also been presented [12–14]. In these experiments, the test of BCP is extended to a more general matter-wave and matter-particle domain. In some recent experiments, with single photons and single atoms [10,11,14], the space-like separation between the measurement selection and the moment when the particle enters the interferometer is achieved, which radically precludes the existence of a local hidden variable.

A conceptually different type of delayed-choice experiment was recently suggested [15] in which BS_2 is replaced by a quantum-controlled BS. The BS can be manipulated in a superposition state of presence and absence which correlates to a superposition state $\cos\theta|0\rangle_a + \sin\theta|1\rangle_a$ of an ancilla. The circuit representation of the experiment is shown in Fig. 1(b), where the BS is represented by Hadamard gate. In such an experimental setup, both of the measurement arrangements exist simultaneously and, thus, the wave-like and particle-like behaviors of the input particle can be tested at the same time. The superposition of wave-like and particle-like behaviors entangled with the state of ancilla can be observed. Different from Wheeler's original delayed-choice experiment, in this quantum version of the experiment, the quantum superposition of the two measurement arrangements intrinsically precludes the possibility that the input particle

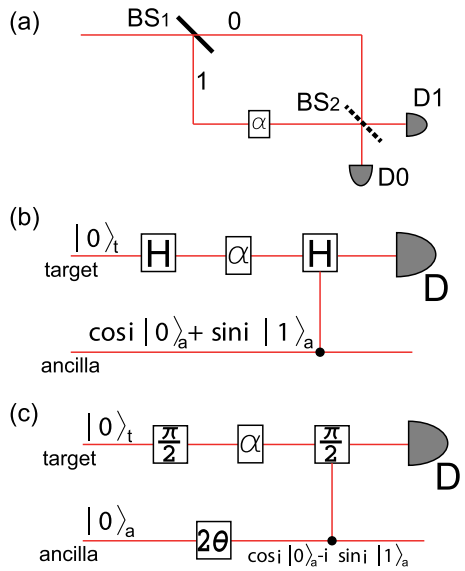

Fig. 1. (a) Schematic of the MZI used in Wheeler's delayed-choice experiment with photons. $BS_{1(2)}$ is the beam splitter, and BS_2 is chosen to exist or be absent to test the wave-like and particle-like behaviors, respectively. α is the phase lag between the two paths 0 and 1, and the final output is detected by two single-photon detectors D0 and D1. (b) Circuits representation of a QDC experiment with the MZI, where the function of the BS is shown as a Hadamard gate and the second Hadamard gate is controlled by an ancilla qubit. (c) Circuit representation of a QDC experiment with neutral atoms in RI. Both the target and ancilla atoms are initially prepared in $|0\rangle$, and the $\pi/2$-rotations are used to separate and recombine the target atom. The second $\pi/2$-rotation is controlled by the internal states of the ancilla atom through Rydberg-Rydberg interaction with the target atom. The state of the ancilla atom is generated by a 2θ-rotation from initial state $|0\rangle_a$. In both (b) and (c), D means the corresponding detection system.

knows which measurement setup it will encounter. The space-like separation between the measurement selection and the moment of the particle's entrance of the interferometer in Wheeler's discussion is no longer a prerequisite. What is more, one can choose the wave-like or particle-like behavior of the input particle after it has been detected by measuring the state of the ancilla. This gives a new interpretation of BCP with a complementarity of experimental data rather than a complementarity of experimental setups. This enriches our understanding of the behaviors of quantum particles and makes the experimental implementation of the QDC very important to the foundation of quantum mechanics. The key point of implementing the QDC experiment is to find the corresponding quantum BS for different particles. Up to now, the QDC experiments have been implemented with various systems, such as nuclear magnetic resonance (NMR) [16,17], single photons [18–20], and single quantum circuits [21]. Different from the experiment with massless photons, the experiments with NMR and single quantum circuits are on some elementary particles, such as the hydrogen nuclear (actually the proton) and electron, and the results are in perfect accordance with the theory. Here we present a proposal that uses the Rydberg blockade mechanism to realize the quantum BS for neutral atoms and, thus, extend the experimental realization of the QDC to neutral atoms, such as alkali atoms like the rubidium and cesium atoms. This is a very important improvement over the former experiments. The test of the wave-particle property of these heavy neutral atoms by the QDC experiment is significant not only to understand the BCP in matter-wave and matter-particle domain, but also to the perspective of the quantum information process with neutral atoms [4].

Different from the MZI in the experiments with photons, here we also use a Ramsey interferometer (RI) with single optically trapped neutral atoms [22]. The RI is equivalent to the MZI [21,23], and the $\pi/2$-rotations in the RI correspond to the BSs in the MZI. The individual atoms can be obtained by using a micro-sized far-off resonant trap (FORT) to directly load from a pre-cooling atomic ensemble in a magneto-optical trap (MOT). Due to the light-assisted collision in the micro-sized FORT, only one or no atom will be finally prepared [24–29]. Once single atom with a certain temperature is captured by the FORT; thus, its motion is determined by its initial coordinates and momentum. The motion can be described by the dynamics of a three-dimensional classical harmonic oscillator, and the moving path is then determined by its internal state. Here we define two paths $|0\rangle$ and $|1\rangle$ with two clock states, say $|0\rangle \equiv |6S_{1/2}F = 2, m_F = 0\rangle$ and $|1\rangle \equiv |6S_{1/2}F = 1, m_F = 0\rangle$, if ^{87}Rb is adopted. The atom is initially prepared in $|0\rangle$. By using the first $\pi/2$-rotation, which can be realized by a microwave pulse or two-photon Raman process, the atomic path is split into the superposition of the two paths $|0\rangle$ and $|1\rangle$, and the overall state can be expressed by

$$|\psi\rangle = (|0\rangle - i|1\rangle)/\sqrt{2}. \quad \textbf{(1)}$$

After a certain time T of free evolution, the wave-like or particle-like behavior can be chosen to observe by applying or neglecting the second $\pi/2$-rotation.

By applying the second $\pi/2$-rotation, the test of wave-like behavior is selected. The phase lag $\alpha = \delta_{ac}T$ between these two paths can be tuned by changing the time interval T between the two $\pi/2$-rotations, where δ_{ac} is the differential ac stark shift between $|0\rangle$ and $|1\rangle$ due to the FORT beam. By examining the atom's population in state $|0\rangle$ or $|1\rangle$, the interference fringe with a sinusoidal function of T can be obtained, and this gives the wave-like behavior of the atom. If the second $\pi/2$-rotation is absent, the test of particle-like behavior is selected. By examining the atom's population in $|0\rangle$ or $|1\rangle$, we could get only a probability of $1/2$ on each state, which reflects the particle-like behavior of the atom.

The circuit of the QDC experiment is shown in Fig. 1(c), in which the quantum-controlled $\pi/2$-rotation can be realized by using the Rydberg blockade effect between an ancilla atom and the target atom [30,31]. Suppose we have two optical FORTs adjacent to each other [see Fig. 2(a)]. The distance between the two FORTs is set in a range where a large Rydberg blockade effect exists, for example 10 μm, as in references [30,32,33]. Here the Rydberg state $|r\rangle$ is involved in both of the two atoms, and both of them are initially prepared in $|0\rangle$. As shown in Fig. 2(b), an ancilla-controlled $\pi/2$-rotation on the target atom between states $|0\rangle_t$ and $|1\rangle_t$ can be realized by pulses 3–7 which are sequentially applied in time. When the ancilla atom is in state $|0\rangle_a$, pulses 3 and 7 are far-detuned and have no effect on the target atom. Through pulses 4–6, an equivalent $\pi/2$-rotation on the target atom between $|0\rangle_t \leftrightarrow |1\rangle_t$ is realized via the Rydberg state $|r\rangle_t$. Then the atom state [Eq. (1)] after this equivalent $\pi/2$-rotation in RI is

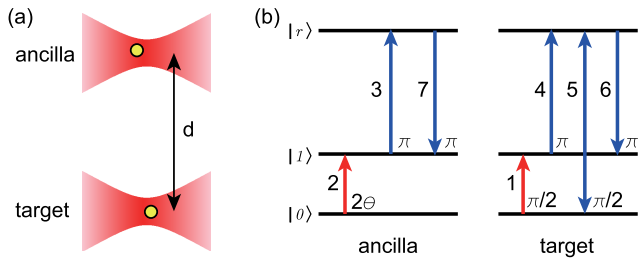

Fig. 2. (a) Schematic of two FORTs with single neutral atoms trapped, in which the distance between them is controlled so that the effective Rydberg blockade exists. (b) Protocols to realize the quantum-controlled $\pi/2$-rotation through Rydberg-Rydberg interaction. The red arrows stand for the rotations between ground states $|0\rangle$ and $|1\rangle$, whereas the blue arrows represent corresponding π- or $\pi/2$-rotations between ground states and Rydberg state $|r\rangle$.

$$|\psi\rangle_w = e^{i\phi}(\cos\phi|0\rangle_t + i\sin\phi|1\rangle_t), \tag{2}$$

where the phase difference between the two paths is $\phi = \frac{\alpha}{2} + \frac{\pi}{4}$ with α being the phase lag between the two paths. The probability of the atom in state $|0\rangle_t$ ($|1\rangle_t$) is then $P_{w,0} = \cos^2\phi$ ($P_{w,1} = \sin^2\phi$), which is a wave-like interference pattern, and the value changes with T. When the ancilla atom is in state $|1\rangle_a$, the pulse 3 excites it to Rydberg state $|r\rangle_a$; thus, the pulses 4–6 will have no effect on the target atom due to the big Rydberg blockade energy shift. Pulse 7 will finally bring the ancilla atom back to state $|1\rangle_a$. The final state of the target atom in this case is then

$$|\psi\rangle_p = (|0\rangle_t - e^{i2\phi}|1\rangle_t)/\sqrt{2}. \tag{3}$$

The probabilities of the atom in both $|0\rangle_t$ and $|1\rangle_t$ are $P_{p,0} = P_{p,1} = 1/2$, and this gives a particle-like behavior.

Now the ancilla atom is prepared into a superposition state $\cos\theta|0\rangle_a - i\sin\theta|1\rangle_a$ by a 2θ-rotation associated with pulse 2. Pulse 2 is intentionally applied after pulse 1 in a time sequence to preclude any possibility that the target atom knows information about the ancilla atom in advance. The overall final state of the circuit in Fig. 1(c) is then an entangled state:

$$|\Psi\rangle_F = \cos\theta|0\rangle_a|\psi\rangle_w - i\sin\theta|1\rangle_a|\psi\rangle_p. \tag{4}$$

The probability of finding the target atom in $|0\rangle_t$ is

$$\begin{aligned} P_0 &= P_{w,0}\cos^2\theta + P_{p,0}\sin^2\theta \\ &= \cos^2\phi\cos^2\theta + \frac{1}{2}\sin^2\theta, \end{aligned} \tag{5}$$

and the probability of an atom in $|1\rangle_t$ is $P_1 = 1 - P_0$. Figure 3 (upper yellow surface) shows the change of P_0 versus the alternations of T and θ. We can see a morphing behavior of the measurement data: the interference pattern with visibility $\mathcal{V} = \cos^2\theta$ is continuously varying between particle ($\theta = \pi/2$) and wave ($\theta = 0$).

The experimental implementation of the fore-mentioned proposal requires a system with two well-controlled single atoms within a Rydberg blockade radius and the good addressability for each atom. Fortunately, current technologies have fulfilled these requirements. For example, the related experimental setup and technology have been used to realize the controlled-NOT quantum gate between two single atoms via the Rydberg blockade effect [32–34]. The only difference

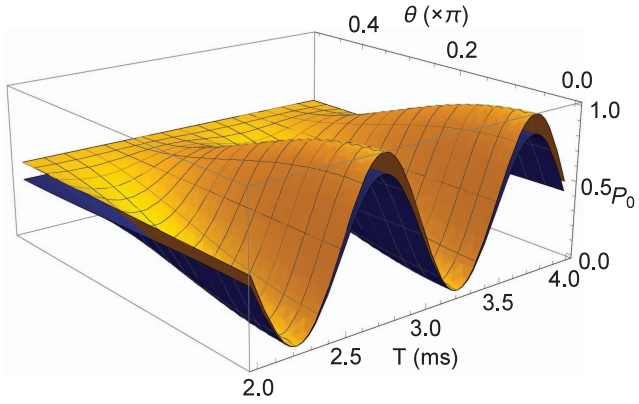

Fig. 3. Morphing behavior of a neutral atom in a QDC experiment. The upper yellow surface is the result without counting any experimental imperfections, whereas the lower blue surface is the expected result with realistic experimental efficiencies. The interference pattern obtained by tuning time interval T is continuously varying between particle ($\theta = \pi/2$) and wave ($\theta = 0$) by altering θ. The differential light shift between $|0\rangle_t$ and $|1\rangle_t$ is set as $2\pi \times 1$ kHz.

here in the QDC experiment is an ancilla-dependent $\pi/2$ phase rotation on a target atom instead of π phase rotation. The ultimate accuracy of the rotation is limited by the Rydberg state lifetime and the Rydberg blockade shift [35,36]. From [34], we see that the best achieved gate can produce a two-atom entangled state with a Bell state fidelity of 0.73. The average success probability of ancilla-controlled p-rotation is $p_0 = 0.87$ ($p_1 = 0.76$) when ancilla is in $|0\rangle$ ($|1\rangle$), without correcting for the atom loss. If we take these numbers as the corresponding success probabilities of our $\pi/2$-rotation, we can then simulate the result of an actual QDC experiment. By taking this into account, the probability of finding the target atom in $|0\rangle_t$ is

$$\begin{aligned} P_0 &= p_0 P_{w,0}\cos^2\theta + p_1 P_{p,0}\sin^2\theta \\ &= p_0\cos^2\phi\cos^2\theta + \frac{p_1}{2}\sin^2\theta. \end{aligned} \tag{6}$$

The corresponding evolution of P_0 versus T and θ is also shown in Fig. 3 (lower blue surface) where the characteristic morphing behavior of a single atom could still be well revealed with a lower amplitude of P_0 and lower visibility (when $0 < \theta < \pi/2$) due to expected experimental imperfections.

Recently, an improved delayed choice experimental scheme has been proposed by Ionicioiu *et al.* [37], where the control ancilla particle is replaced by two space-like separated entangled particles, and one of them is used to control the state of the second BS in the interferometer. By using such a scheme, the hidden variable theories can be checked in the context of wave-particle duality instead of by the commonly used Bell-type experiment. Our proposal is flexible to be directly expanded and implemented by introducing a pair of long-distance entangled neutral atoms, which has also been realized in recent experiments [38,39].

In conclusion, we have presented a proposal to implement the QDC experiment with single neutral atoms via the Rydberg-Rydberg interaction. In such an experiment, the target atom's wave-like and particle-like sates are entangled with the ancilla atom's internal state [see Eq. (4) with $0 < \theta < \pi/2$], which is intrinsically a quantum phenomenon and cannot

be interpreted by classical theory. This point is different from the experiments with photons where rigorous verification of quantum entanglement between the ancilla photon and target photons is needed [19,20]. Moreover, the atom used in our proposal is a FORT trapped atom directly loaded from a MOT, where the energy of the atom is much higher than the quantum energy of the trap, and the spread of the energy covers many vibrational states [40]. Thus, the motion of the atom is mostly like a classical oscillator with a very small matter wave package. The two paths $|0\rangle$ and $|1\rangle$ that the atom follows in FORT are actually two matter wave packages with different atomic spins. Although they are not spatially separated, they experience different energy potential during the atom's oscillation in the FORT, and their interference reflects the behavior of matter waves.

Funding. National Key Research and Development Program of China (2017YFA0304502); National Natural Science Foundation of China (NSFC) (11574187, 11634008, 11674203, 61227902).

REFERENCES AND NOTE

1. N. Bohr, in *Quantum Theory and Measurement*, J. A. Wheeler and W. H. Zurek, eds. (Princeton University, 1984), pp. 9–49.
2. M. O. Scully, B.-G. Englert, and H. Walther, Nature **351**, 111 (1991).
3. B.-G. Englert, Phys. Rev. Lett. **77**, 2154 (1996).
4. X.-S. Ma, J. Kofler, and A. Zeilinger, Rev. Mod. Phys. **88**, 015005 (2016).
5. J. A. Wheeler, in *Mathematical Foundations of Quantum Theory*, A. R. Marlow, ed. (Academic, 1978), pp. 9–48.
6. J. A. Wheeler, in *Quantum Theory and Measurement*, J. A. Wheeler and W. H. Zurek, eds. (Princeton University, 1983), pp. 182–213.
7. A. J. Leggett, in *Compendium of Quantum Physics*, D. Greenberger, K. Hentschel, and F. Weinert, eds. (Springer, 2009), pp. 161–166.
8. T. Hellmuth, H. Walther, A. Zajonc, and W. Schleich, Phys. Rev. A **35**, 2532 (1987).
9. Y.-H. Kim, R. Yu, S. P. Kulik, Y. Shih, and M. O. Scully, Phys. Rev. Lett. **84**, 1 (2000).
10. V. Jacques, E. Wu, F. Grosshans, F. Treussart, P. Grangier, A. Aspect, and J.-F. Roch, Science **315**, 966 (2007).
11. X.-S. Ma, S. Zotter, J. Kofler, R. Ursin, T. Jennewein, C. Brukner, and A. Zeilinger, Nat. Phys. **8**, 479 (2012).
12. B. J. Lawson-Daku, R. Asimov, O. Gorceix, C. Miniatura, J. Robert, and J. Baudon, Phys. Rev. A **54**, 5042 (1996).
13. T. Kawai, T. Ebisawa, S. Tasaki, M. Hino, D. Yamazaki, T. Akiyoshi, Y. Matsumoto, N. Achiwa, and Y. Otake, Nucl. Instrum. Methods Phys. Res., Sect. A **410**, 259 (1998).
14. A. G. Manning, R. I. Khakimov, R. G. Dall, and A. G. Truscott, Nat. Phys. **11**, 539 (2015).
15. R. Ionicioiu and D. R. Terno, Phys. Rev. Lett. **107**, 230406 (2011).
16. S. S. Roy, A. Shukla, and T. S. Mahesh, Phys. Rev. A **85**, 022109 (2012).
17. R. Auccaise, R. M. Serra, J. G. Filgueiras, R. S. Sarthour, I. S. Oliveira, and L. C. Céleri, Phys. Rev. A **85**, 032121 (2012).
18. J.-S. Tang, Y.-L. Li, X.-Y. Xu, C.-F. Xiang, G.-Y. Li, and G.-C. Guo, Nat. Photonics **6**, 600 (2012).
19. A. Peruzzo, P. Shadbolt, N. Brunner, S. Popescu, and J. L. O'Brien, Science **338**, 634 (2012).
20. F. Kaiser, T. Coudreau, P. Milman, D. B. Ostrowsky, and S. Tanzilli, Science **338**, 637 (2012).
21. S.-B. Zheng, Y.-P. Zhong, K. Xu, Q.-J. Wang, H. Wang, L.-T. Shen, C.-P. Yang, J. M. Martinis, A. N. Cleland, and S.-Y. Han, Phys. Rev. Lett. **115**, 260403 (2015).
22. Z. Wang, Y. Tian, C. Yang, P. Zhang, G. Li, and T. Zhang, Phys. Rev. A **94**, 062124 (2016).
23. H. Lee, P. Kok, and J. P. Dowling, J. Mod. Opt. **49**, 2325 (2002).
24. N. Schlosser, G. Reymond, I. Protsenko, and P. Grangier, Nature **411**, 1024 (2001).
25. N. Schlosser, G. Reymond, and P. Grangier, Phys. Rev. Lett. **89**, 023005 (2002).
26. T. Grunzweig, A. Hilliard, M. McGovern, and M. F. Andersen, Nat. Phys. **6**, 951 (2010).
27. A. V. Carpentier, Y. H. Fung, P. Sompet, A. J. Hilliard, T. G. Walker, and M. F. Andersen, Laser Phys. Lett. **10**, 125501 (2013).
28. P. Sompet, A. V. Carpentier, Y. H. Fung, M. McGovern, and M. F. Andersen, Phys. Rev. A **88**, 051401 (2013).
29. B. J. Lester, N. Luick, A. M. Kaufman, C. M. Reynolds, and C. A. Regal, Phys. Rev. Lett. **115**, 073003 (2015).
30. E. Urban, T. A. Johnson, T. Henage, L. Isenhower, D. D. Yavuz, T. G. Walker, and M. Saffman, Nat. Phys. **5**, 110 (2009).
31. A. Gaetan, Y. Miroshnychenko, T. Wilk, A. Chotia, M. Viteau, D. Comparat, P. Pillet, A. Browaeys, and P. Grangier, Nat. Phys. **5**, 115 (2009).
32. L. Isenhower, E. Urban, X. L. Zhang, A. T. Gill, T. Henage, T. A. Johnson, T. G. Walker, and M. Saffman, Phys. Rev. Lett. **104**, 010503 (2010).
33. X. L. Zhang, L. Isenhower, A. T. Gill, T. G. Walker, and M. Saffman, Phys. Rev. A **82**, 030306 (2010).
34. K. M. Maller, M. T. Lichtman, T. Xia, Y. Sun, M. J. Piotrowicz, A. W. Carr, L. Isenhower, and M. Saffman, Phys. Rev. A **92**, 022336 (2015).
35. M. Saffman, T. G. Walker, and K. Mølmer, Rev. Mod. Phys. **82**, 2313 (2010).
36. M. Saffman and T. G. Walker, Phys. Rev. A **72**, 022347 (2005).
37. R. Ionicioiu, T. Jennewein, R. B. Mann, and D. R. Terno, Nat. Commun. **5**, 3997 (2014).
38. J. Hofmann, M. Krug, N. Ortegel, L. Gérard, M. Weber, W. Rosenfeld, and H. Weinfurter, Science **337**, 72 (2012).
39. W. Rosenfeld, D. Burchardt, R. Garthoff, K. Redeker, N. Ortegel, M. Rau, and H. Weinfurter, Phys. Rev. Lett. **119**, 010402 (2017).
40. For instance, if a 1064 nm FORT beam is focused to a radial size of 3 μm with a trap depth of $\mathrm{lm}\,K \times k_B$ for the $^{87}\mathrm{Rb}$ atom, the corresponding vibrational quantum energies are then $E_r = 1.6\ \mu\mathrm{K} \times k_B$ on radial direction and $E_a = 0.13\ \mu\mathrm{K} \times k_B$ on axial direction. The typical temperature of an atom directly loaded from a MOT is around 100 μK, which is much larger than E_r and E_a. What is more, the energy variance of the atom in Boltzmann distribution is about 120 μK and covers more than 75 vibrational states. The corresponding de Broglie wavelength of the atom is about 19 nm.